Applied Catalysis B: Environmental 338 (2023) 123046

Contents lists available at ScienceDirect

Applied Catalysis B: Environmental

journal homepage: www.elsevier.com/locate/apcatb

Improved electrocatalytic activity of Pt on carbon nanofibers for glucose oxidation mediated by support oxygen groups in Pt perimeter

M.P.J.M. Van der Ham [a,b], T.J.P. Hersbach [c,1], J.J. Delgado [d], B.D. Matson [c,2], J. Lim [c,3], M. Führer [a], T. Van Haasterecht [a], M.W.G.M. Verhoeven [e], E.J.M. Hensen [e], D. Sokaras [c], M.T.M. Koper [b], J.H. Bitter [a,*]

[a] Wageningen University & Research, Biobased Chemistry and Technology, P.O. Box 17 6700 AA Wageningen, the Netherlands
[b] Leiden Univcrsity, Catalysis and Surface Chemistry, P.O. Box 9502 2300 RA, the Netherlands
[c] SLAC National Accelerator Laboratory, 2575 Sand Hill Rd, Menlo Park, CA, United States
[d] University of Cádiz, Material Science and Metallurgy Engineering and Inorganic Chemistry, 11510 Puerto Real, Cadiz, Spain
[e] Eindhoven University of Technology, Chemical Engineering and Chemistry, PO Box 513 5600 MB, the Netherlands

ARTICLE INFO

Keywords:
Pt on carbon nanofibers
Support oxygen groups
Electrocatalytic oxidation of glucose
Catalyst design
Perimeter

ABSTRACT

Support effects in supported metal catalysts are well studied for thermocatalytic reactions, but less studied for electrocatalytic reactions. Here, we prepared a series of Pt supported on carbon nanofiber catalysts which vary in their Pt particle size and the content of oxygen groups on the surface of the CNF. We show that the activity of these catalysts for electrocatalytic glucose oxidation relates linearly with the content of support oxygen groups. Since the electronic state of Pt (XAS) and Pt surface structure (CO-stripping) were indistinguishable for all materials, we conclude that sorption effects of glucose play a crucial role in catalytic activity. This was further confirmed by establishing a relation between the annulus of the Pt particles and the activity.

1. Introduction

The most promising method for the oxidation of saccharides to various carboxylates is through stoichiometric processes (*e.g.*, with nitric acid), despite the moderate selectivity and emission of hazardous NO_x compounds [1,2]. The development of a green and sustainable production route for the selective oxidation of saccharides has therefore gained great interest. In this regard, electrocatalytic processes have attracted increasing attention, as they can operate under mild reaction conditions (room temperature, neutral pH) and do not require hazardous redox agents [2]. Moreover, in paired electrolysis, the oxidation of saccharides at the anode can be achieved at low potentials and consequently reduce the energy input for hydrogen evolution or CO_2 reduction at the cathode [3–6]. These advances in paired electrolysis are promising for cogenerating energy carriers and value-added platform chemicals, yet significant further steps need to be made to improve the heterogeneous electrocatalyst performance at the anode to bring paired electrolysis for large-scale chemical production a step closer to reality.

There are two distinct approaches to improving the electrocatalyst performance, namely by tuning the properties of the supported catalyst or the properties of the support itself. The former can be tuned by tweaking, among others, the catalyst particle size [7], modifying the catalyst surface structure [8,9], encapsulating the catalyst within a polymer layer [10], adding ad-atoms [9] or changing the type of metal [8,11]. The second approach involves changing the type of support [12], modifying the support morphology [13], doping the support with hetero-atoms [14], introducing support functionalities [15]. Support functionalities have been widely studied, especially in the field of thermocatalysis, where it has been shown that they can induce various effects on the catalyst properties and consequently its performance [16].

Thermocatalytic studies have shown that support functionalities can affect the catalyst performance *via* multiple mechanisms. For example, support functionalities have been shown to affect the support polarity and thus influence the adsorption/desorption rate and the adsorption

* Corresponding author.
E-mail address: harry.bitter@wur.nl (J.H. Bitter).
[1] ORCID: 0000–0001-5467–6151
[2] ORCID: 0000–0001-5733–0893
[3] ORCID: 0000–0002-1875–659X

https://doi.org/10.1016/j.apcatb.2023.123046
Received 1 February 2023; Received in revised form 19 June 2023; Accepted 24 June 2023
Available online 28 June 2023

mode of the reactant on the active phase of the supported catalyst [17–21]. Thereby, it affects the catalyst activity and selectivity, as was shown for the dehydrogenation of cinnamaldehyde over Pt on carbon nanofibers upon removal of acidic support groups [17,18]. Besides, functional groups on carbon supports can change the electron density of the supported catalyst [22]. Similar results were obtained for doping carbon supports with various elements [23]. This change in electron density of the supported catalyst changes in its turn the adsorption/-desorption rate of reactants, consequently altering the catalyst performance [22,23].

On the other hand, support functionalities can play a crucial role in catalytic reactions, as was shown for bifunctional catalysis [24,25], cooperative catalysis [26,27], and hydrogen spillover [28]. Bifunctional catalysis on metal-baring carbon supports can occur when support functionalities have their own catalytic role in the chemical reaction [24,25,29]. In contrast, in cooperative catalysis, the support functionalities can function as a promotor. The promotor can reduce the activation energy barrier of the rate-limiting step, thereby improving the catalyst activity [26,30]. An increase in hydrogen spillover was related to a higher content of quinone groups on the Co/CNT catalyst support and consequently improved the catalyst for Fischer-Tropsch synthesis [28].

In contrast to this wealth of thermocatalytic studies, the field of electrocatalysis has yielded fewer studies elucidating the role of support functionalities on the performance of supported electrocatalysts [16]. Some effects induced by support functionalities on the electrocatalyst performance have been attributed to a change in charge transfer resistance for heteroatom-doped carbon [31], a change in proton conductivity and wettability for sulfonated carbon [32], and an improved adsorption of reactants for nitrogen functionalized carbon [33]. More studies have attempted to elucidate the effect of support oxygen groups on the performance of supported electrocatalysts [34–39]. However, these studies were less systematic, as the support oxygen groups have been modified by (harsh) acid or gas-phase treatments before impregnation [34–39]. This does not only result in the modification of the type and content of support oxygen groups but also other properties of the support and the supported catalyst properties. These multiple modifications made it impossible to relate the effect of support oxygen groups on the catalytic performance of the catalyst.

Therefore, the purpose of the study is to evaluate the effect of support oxygen groups on the performance of supported electrocatalysts, by comparing self-synthesized Pt/CNF catalysts with different types and contents of support oxygen groups and by studying how these support-oxygen groups affect the catalyst activity towards the oxidation of glucose. Additionally, *in-situ* XANES, *ex-situ* XPS, and CO-stripping are performed to determine how these support oxygen groups affect the performance of the supported electrocatalyst.

2. Experimental section

2.1. Preparation of carbon nanofibers (CNF)

Ni/SiO_2 to be used for the CNF growth (5 wt% Ni) was synthesized *via* homogeneous deposition precipitation based on a protocol described by Dillen et al.[40] A slurry of 20 g silica (aerosol 300, Evonik), 5.23 g nickel(II) nitrate hexahydrate (Sigma-Aldrich) and 3.23 g urea (Acros) in 1 L miliQ (MQ) water was acidified to pH = 3 with 68% HNO_3 (Merck). The slurry was then stirred at 850 rpm for 18 h at 363 K to yield a gel. The gel was washed three times with MQ water before drying in static air at 383 K for 18 h. The collected material was crushed with a mortar and pestle and sieved to obtain 425–800 μm particles. The resulting material was subsequently calcined in static air at 873 K for 18 h, yielding NiO/SiO_2.

The NiO/SiO_2 was used to synthesize CNF as described by Toebes et al.[17] 3 g of NiO/SiO_2 were placed in a quartz boat in a tubular oven and reduced to Ni/SiO_2 at 1 bar and 973 K in 240 $ml.min^{-1}$ N_2 and 60 $ml.min^{-1}$ H_2 for 2 h (heating ramp 5 $K.min^{-1}$). After cooling to 823 K the gas flow was switched to 38 $ml.min^{-1}$ H_2, 100 $ml.min^{-1}$ CO and 168 $ml.min^{-1}$ N_2 for 26 h to grow the CNF. The obtained material was washed three times with 1 M KOH to remove the SiO_2. This synthesis methodology by chemical vapor deposition yields high purity CNF supports that are uniform in their porosity, are mesoporous and have a high surface area [41,42]. After washing with water, the material was refluxed in 68% HNO_3 for 1.5 h to remove exposed Ni and introduce oxygen-containing groups on the CNF surface, yielding a CNF-ox support. The support material was crushed with a mortar and pestle and sieved to obtain a 90–210 μm particle size fraction, which was used for impregnation.

2.2. Impregnation of CNF with Pt

Incipient wetness impregnation was used to load 5 wt% of Pt on the CNF-ox support. Tetraamine platinum(II) nitrate ($[Pt(NH_3)_4](NO_3)_2$) (Merck) was dissolved in MQ and added dropwise to the support to incipient wetness. In between additions, the sample was vigorously mixed. After impregnation, the catalyst was dried at 383 K and successively calcined at 523 K for 2 h to yield the PtO_x/CNF-ox catalyst.

2.3. Removal of surface oxygen-containing groups

Pt/CNF catalysts with different amounts of surface oxygen-containing groups were prepared by heat treatments at different temperatures. First, PtO_x/CNF-ox (1.0 g) was placed in a quartz boat inside a tubular oven. The oven tube was flushed with H_2/N_2 (100 ml $H_2.min^{-1}$ and 209 $ml.min^{-1}$ N_2) for 30 min and heated to 523 K for 2 h (heating ramp 5 $K.min^{-1}$) to reduce the catalyst. The resulting catalyst is denoted as Pt/CNF-R523. The reduced catalyst was then heat treated in a N_2 flow of 266 $ml.min^{-1}$ for 2 h at 573 K or 773 K or 973 K (heating ramp 5 $K.min^{-1}$), generating Pt/CNF-R573, Pt/CNF-R773, and Pt/CNF-R973, respectively. Finally, the catalysts were ground to a fine powder < 75 μm with a mortar and pestle.

2.4. Electrode preparation

A glassy carbon electrode (GCE) was used as support. The GCE was polished successively with 3 and 1 μm diamond polish (Buehler) to a mirror finish [43]. Between steps the GCE was sonicated successively in MQ and ethanol and finally washed thoroughly with MQ to remove any organic and inorganic material. After these treatments, the GCE weight was determined accurately on a microbalance. Next, a catalyst ink was prepared by suspending 50 mg Pt/CNF in 200 μL Nafion 1100 W (Sigma-Aldrich, 5 wt% in lower aliphatic alcohols and water) and 800 μL anhydrous THF (Merck). 30 μL of catalyst ink was drop cast on the GCE. The electrode was air-dried for 5 min and oven dried for another 10 min at 333 K and weighed again (aiming at a 1.5 ± 0.15 mg loading).

2.5. Electrochemical oxidation of Pt/CNF

The effect of electrochemical oxidation of the support of Pt/CNF-R523, Pt/CNF-R773 and Pt/CNF-R973 was studied by holding the potential at 1.4 V *vs.* RHE for 30 min in 0.1 M H_2SO_4, generating Pt/CNF-R523-EO, Pt/CNF-R773-EO and Pt/CNF-R973-EO (EO = electrochemically oxidized). After this electrochemical glucose oxidation experiments were performed below at $E \leq 1.0$ V *vs.* RHE to avoid the electrochemical oxidation of the CNF support, since the electrochemical oxidation of amorphous and graphitic carbon starts at 0.95 V [44] and 1.2 V *vs.* RHE [45], respectively. Moreover, Pt can accelerate the electrochemical oxidation of graphitic carbon in its annulus [46,47].

2.6. Catalyst characterization

N_2-physisorption was performed at 77 K using a Micromeritics

Tristar II Plus to determine the BET surface area, pore volume, and average pore size. The samples were vacuum-dried at 373 K for 2 h before analysis.

Temperature-programmed decomposition coupled to a mass spectrometer (TPD-MS) was performed with a Micromeritics Autochem II 2920 to qualitatively determine the functional groups (surface oxygen-containing groups) of the synthesized catalysts. 100 mg of catalyst was heated to 1173 K at 10 K.min^{-1} under 20 ml.min^{-1} He gas flow. The gasses were analyzed with a THERMOStarTM mass spectrometer from Pfeiffer.

The content of oxygen groups was determined by thermogravimetric analysis (TGA) using a Mettler Toledo TGA/DSC 1. 50 mg of catalyst was placed in a 70 μl alumina crucible and exposed to a 130 ml.min^{-1} N_2 flow. As a reference a N_2 flow of 20 ml.min^{-1} was used. The temperature program consisted of a 5 K.min^{-1} ramp to 373 K, an isothermal period of 30 min followed by a ramp of 5 K.min^{-1} to 1173 K, and a final isothermal period of 5 min. The thermogravimetric curves were processed to obtain the derivative of the thermogravimetric curve (DTG) and used for comparison with TPD-MS data.

X-ray diffraction (XRD) measurements were recorded with a Bruker D8 Advance to characterize the graphitic nature of the CNF support. The system was equipped with an Lynxeye-XE-T PSD detector and a Cu-K$\alpha_{1,2}$ tube generating X-rays with $\lambda = 1.542$ Å. The scans were recorded from $2\theta = 10^\circ$ to $2\theta = 90^\circ$ with a step size of 0.05° [48].

The Pt loading was quantified thermogravimetrically using the same Mettler Toledo TGA/DSC by complete combustion of the carbon support in air (80 ml.min^{-1}) with a reference gas flow of 20 ml.min^{-1} and temperature program of a ramp of 10 K.min^{-1} to 373 K, an isotherm of 30 min and a ramp of 10 K.min^{-1} to 1173 K. At 1173 K and under air Pt is retained in its metallic state with few oxygen species (5–10%) on the grain boundaries and defective sites [49].

X-ray photoelectron spectroscopy (XPS) analysis was performed with a Thermo Scientific K-Alpha, equipped with a 180° double-focusing hemispherical analyzer, a 128-channel detector, and a monochromatic small-spot X-ray source. The spectra were collected at a spot size of 400 μm with an aluminum anode (Al Kα=1486.6 eV) operated at 72 W. The data were analyzed with CasaXPS. Two different approaches were used for the wide scans and narrow scans. The wide scans were measured at 200 eV to determine the atomic composition of the Pt/CNF catalysts. For the wide scans, the samples were reduced first in a plug flow reactor at 523 K while keeping it in place with quartz wool (SiO_2) for 2 h under a 209 ml.min^{-1} N_2 flow and a 100 ml.min^{-1} H_2 flow to remove chemisorbed water [50]. The $Pt_{4\,f}$ and $O_{1\,s}$ arrow scans were measured at 50 eV to identify the Pt oxidation state present on the support and to determine the relative contribution of different types of support oxygen groups present on the support. For the narrow scans, the samples were characterized without pretreatment to avoid the contamination of the O1s peak with SiO_2.

All the samples were characterized by high resolution transmission electron microscopy (HRTEM) and scanning transmission electron microscopy-high angle annular dark field (STEM-HAADF) using an aberration-corrected FEI Titan^3 Themis 60–300 microscope. The Pt particle size distribution was obtained by counting a minimum of 100 particles. Both the number average Pt particle size and the surface area average Pt particle size were used.

The specific capacitance of the Pt/CNF, an indicator for the content of support oxygen groups, was characterized by cyclic voltammetry (CV) [51]. The CVs were recorded between 0.1 and 1.0 V in 0.1 M H_2SO_4 (Merck, Suprapur) solutions at a scan rate of 5 mV.s^{-1}. All electrochemical measurements were performed at room temperature and under oxygen-free conditions in a three-electrode glass cell in which the reference was a RHE, separated from the work compartment by a Luggin capillary [52]. The specific capacitance was calculated from the CV curve according to the following equation [53,54]:

$$C = \frac{\int IEdE}{vm\Delta E}$$

I (A) and E (V) are the current measured and applied potential during the CV, v (V.s^{-1}) is the scan rate, m is the mass of the Pt/CNF loaded on the GCE and ΔE is the potential window of interest [51].

CO-stripping from Pt/CNF was performed both to clean the catalyst surface from any possible contaminants and to measure the electrochemical surface area (ECSA) of the prepared electrocatalysts before testing their catalytic performance. CO-stripping was performed in 0.1 M H_2SO_4 (pH = 1) by holding the potential at 0.1 V *vs.* RHE for 30 min while purging the solution with CO to saturate the Pt surface with CO, after which the solution was purged another 30 min with Ar to remove any dissolved CO. Successively 5 CVs were recorded up to 1.0 V to avoid dissolution of Pt [55,56], to avoid restructuring of the Pt particles [55,56], and to prevent the oxidation of the carbon support [45]. The contribution of CO oxidation from other electrochemical processes was differentiated by subtracting the second anodic scan from the first anodic scan [57].

In-situ Pt L_{III}-edge HERFD-XANES spectra were collected at beamline 15–2 of the Stanford Synchrotron Radiation Lightsource using a liquid nitrogen-cooled Si(311) double-crystal monochromator. A configuration of two Rh-coated Kirkpatrick–Baez mirrors delivered at the sample position an incident X-ray beam with a full width at half maximum (FWHM) of ~130 × 860 μm^2 (vertical x horizontal) and a photon flux of ~4 × 10^{12} photons/sec was used. The beam energy was calibrated by assigning a value of 11563.7 eV to the first inflection of a Pt reference metallic foil. The fluorescent X-rays were detected with a high energy resolution using a seven-crystal Johann-type spectrometer [58]. The spectrometer detected the maxima of Pt $L_{\alpha 1}$ emission line at a Bragg angle of ~79.95° and an energy resolution of ~0.8 eV by using seven Ge (660) crystals of 100 mm diameter, spherically bent with a 1-meter radius of curvature. The advantage of this method has been described before.[48].

The aforementioned protocol was used to acquire *operando* spectra in a homemade, 25-ml volume polystyrene electrochemical cell to which a 0.5-mm thick glassy carbon electrode (HTW-Germany, Sigradur G) working electrode was affixed using a 5-mm diameter hole in the side of the cell. The working electrode contained a small amount of catalyst ink, which was prepared by mixing 30 mg catalyst powder with 200 μL Nafion 1100 W (Sigma-Aldrich, 5 wt% in lower aliphatic alcohols and water), 480 μL ethanol (Merck, Uvasol) and 320 μL isopropanol (Sigma-Aldrich, for HPLC). Before each experiment, this catalyst ink was ultrasonicated for 1 min, after which 4 μL was drop cast on the working electrode and air-dried. In addition to this working electrode, the electrochemical cell contained a HydroFlex reversible hydrogen reference electrode (Gaskatel), and a glassy carbon counter electrode (Alfa Aesar, type 1, 5 mm diameter, 100 mm length). Once assembled, the cell was filled with 0.1 M H_2SO_4 (Merck, Suprapur), and the catalyst was cleaned and characterized in a fume hood with carbon monoxide as described in the "Catalyst Characterization" section. Following these steps, the cell was moved to the beamline to collect *in-situ* X-ray absorption spectra at various electrode potentials. The small (sub-0.2 eV) gradual energy drifts of the monochromator occurred along the multiple days of the experimental study and were accurately corrected by aligning a fixed glitch feature of the monochromator crystals throughout all collected spectra. The collected spectra were successively averaged, flattened, and normalized in ATHENA [59]. Because the spectra were normalized by setting the edge jump to 1, all absorption intensities will be reported in units of 'edge fraction' [60].

Using HERFD-XANES, the potential-dependent adsorbate coverage on the Pt electrocatalyst surface was calculated using the spectral features caused by each adsorbate. To do so, four spectral components were defined. The first of these is the spectrum of each catalyst at 0.4 V *vs.* RHE in absence of glucose: this spectrum corresponds as closely as possible to a Pt surface without adsorbates and is therefore referred to as

the 'base spectrum' [61]. The remaining three components are the difference spectra that are obtained by subtracting the base spectrum from another spectrum. Specifically, the *OH adsorbate was defined by subtracting the base Pt spectrum from the spectrum obtained at 0.78 V *vs.* RHE (without glucose present). At this potential, Pt is covered by *OH [61], such that the resulting difference spectra can be taken as the fingerprint for adsorbed *OH. The *glucose adsorbate was defined by subtracting the base Pt spectrum from the spectrum at 0.1 V *vs.* RHE in the presence of 0.1 M glucose. Under these conditions, the Pt surface is likely to be fully covered by *glucose and its decomposition products [62–64]. Therefore, the resulting difference spectrum is a proxy for the coverage of glucose-derived species. Finally, the PtO_x species was defined as the difference spectra taken from Pt at 1.0 V *vs.* RHE (with glucose present), whence the Pt surface is free of adsorbates [64]. The Pt adsorbate coverages were extracted by fitting a combination of the base spectrum, the *OH difference spectrum, the *glucose difference spectrum, and the PtO_x difference spectrum to the experimental XANES spectra. This approach, also known as linear combination analysis (LCA), yields an estimate of the relative coverages of each adsorbate.

2.7. Performance testing

The performance of the catalyst, after CO-stripping (described in the "Catalyst Characterization" section), was studied by linear sweep voltammetry (LSV) and by chronoamperometry (CA) in 0.1 M H_2SO_4. LSV was conducted from 0.1 to 1.0 V *vs* RHE with a scan rate of 1 $mV.s^{-1}$. First a blank (*i.e.*, all components except glucose were present in the reactor) LSV was measured, after which 0.1 M glucose (99.5%, Merck) was added. The system was purged for 30 min with Ar to ensure a homogeneous solution before repeating the LSV with glucose. The currents measured for glucose oxidation reported in this study for LSV are an average of two experiments and have been corrected by the blank for surface charging [65]. A similar procedure was used for CA as was used for LSV, namely a blank measurement, followed by 0.1 M glucose addition, purging the system for 30 min, and another measurement in the presence of glucose.

3. Results & discussion

The results and discussion section has been subdivided into three individual sections that discuss the characterization of the support oxygen groups on the different Pt/CNF catalysts (1) and the characterization of the platinum supported on the carbon nanofiber catalysts (2). These sections were used as a basis to evaluate the performance of the different Pt/CNF catalysts for the electrocatalytic oxidation of glucose (3).

3.1. Characterization of support oxygen groups on different Pt/CNF catalysts

Table 1 shows a summary of the content of support oxygen groups determined by TGA (weight %, see Fig. S1 for details) and XPS (O/C ratios, see Table S1 and Fig. S2 for details) and the number of oxygen groups normalized per surface area (atoms.nm^{-2}, using the BET surface area of 187 $m^2.g^{-1}$ for bare CNF-ox, see Table S2 and Fig. S3 for details) as has been done before [66]. The BET surface area of Pt/CNF-ox and Pt/CNF-R973 are similar (Table S2), indicative that the heat treatment does not affect the surface structure of the synthesized catalysts [67].

TGA shows that the number of support oxygen groups decreased from 6.6 oxygen atoms.nm^{-2} for PtO_x/CNF-ox to 5.0 oxygen atoms.nm^{-2} for Pt/CNF-R523. Successive heat treatment steps resulted in a gradual decrease in support oxygen groups to 1.5 oxygen atoms.nm^{-2} for the sample heat-treated at 973 K which is in line with earlier studies [54,66].

XPS shows a decrease in support oxygen groups from 6.8 oxygen atoms.nm^{-2} for Pt/CNF-R523 to 4.1 oxygen atoms.nm^{-2} for Pt/CNF-973 K. XPS and TGA show a difference in absolute values for the support oxygen groups content, which can be explained by the difference in analytical technique (*e.g.*, probing depth). As a result, XPS is less affected by the decomposable surface oxygen groups [68,69]. Nonetheless, XPS shows a similar trend to that observed by TGA, namely a decrease in support oxygen group content for catalysts exposed to higher thermal treatments.

Table 1
The total number of oxygen groups on the support (O-atoms.nm^{-2}) of the synthesized Pt/CNF catalysts as a function of reduction treatment (Pt/CNF-R523) and heat treatment (Pt/CNF-R523 to Pt/CNF-R973) determined by TGA and XPS and the weight fraction of oxygen groups (wt%) decomposed above 673 K determined by TGA.

Catalyst	TGA			XPS	
	Weight loss (%)		O-atoms. nm^{-2}	O/C atomic ratio	O-atoms. nm^{-2}
	Total	> 673 K	Total	Total	Total
PtO_x/CNF-ox	5.8	4.1 ± 0.1	6.6 ± 0.1	-	-
Pt/CNF-R523	4.4	3.5 ± 0.1	5.0 ± 0.3	0.054	6.8 ± 0.6
Pt/CNF-R573	4.2	3.3 ± 0.0	4.9 ± 0.0	0.037	4.9 ± 0.7
Pt/CNF-R773	3.3	2.6 ± 0.1	3.8 ± 0.4	0.030	3.8 ± 0.6
Pt/CNF-R973	1.3	0.9 ± 0.1	1.5 ± 0.3	0.032	4.1 ± 0.0

The nature of the support oxygen groups on the Pt/CNF catalysts was characterized by TPD-MS (Fig. S4), DTG (Fig. S5), and O_{1s} XPS spectra (Fig. S6 and Table S3). The parent catalyst, PtO_x/CNF-ox, was found to bear carboxylic acids, anhydrides, lactones, phenols and carbonyls/quinones [28,50,54]. After a reduction step at 523 K, the carboxylic acids, anhydrides, carbonyl groups adjacent to ketones and aldehydes are removed [28,50,54], indicative that Pt/CNF-R523 only bares lactone, phenol and carbonyl/quinone surface groups. With an increase in the heat treatment step, the content of lactone, phenol and carbonyl/quinone surface groups is gradually reduced [28,50,54].

The graphitic nature of the bare CNF-ox support and of Pt/CNF-R573 and Pt/CNF-R973 (*e.g.*, subjected to mild and high heat treatment temperatures) was characterized by XRD (Fig. S7). No significant difference was found between the graphitic nature of Pt/CNF-R573 and Pt/CNF-R973, indicative that it was not affected by the heat treatment [48]. The electrochemical properties of the support oxygen groups were studied by CV in 0.1 M H_2SO_4. Fig. 1A shows the weight normalized steady-state CV (the fourth CV after CO-stripping) for the different catalysts. For PtO_x/CNF-ox, in the forward scan, three oxidative peak currents can be observed, while in the backward scan, only two cathodic peak currents can be observed. In the forward scan, peak 1 from 0.1 to 0.3 V *vs.* RHE is attributed to the desorption of hydrogen from Pt [55], while peak 2 from 0.4 to 0.8 V *vs.* RHE represents the oxidation of phenol/hydroquinone surface groups to lactone and carbonyl/quinone groups [54,70], and peak 3 from 0.8 to 1.0 V *vs.* RHE is related to the oxidation of metallic Pt to PtO_x [55]. In the backward scan, peak 4 from 0.8 to 0.4 V *vs.* RHE represents both the reduction of PtO_x to metallic Pt [55] and the reduction of lactone and carbonyl/quinone support oxygen groups to phenol/hydroquinone groups [70], while peak 5 below 0.4 V *vs.* RHE is related to hydrogen adsorption on Pt [55]. The redox reaction of carboxylic acid groups could not be observed from the CV of PtO_x/CNF-ox since the redox potential of these groups is between 1.1 and 1.6 V *vs.* RHE [70]. Thus, from the CVs it can be concluded that all catalysts bare electroactive Pt nanoparticles and redox-active phenol and hydroquinone support oxygen groups, confirming the results obtained by TGA, XPS, and TPD-MS.

The CV in Fig. 1A shows that peak 2 and peak 4 are similar in intensity for PtO_x/CNF-ox and Pt/CNF-R523, thereby indicating that the reduction step at 523 K does not change the content of lactone, phenol

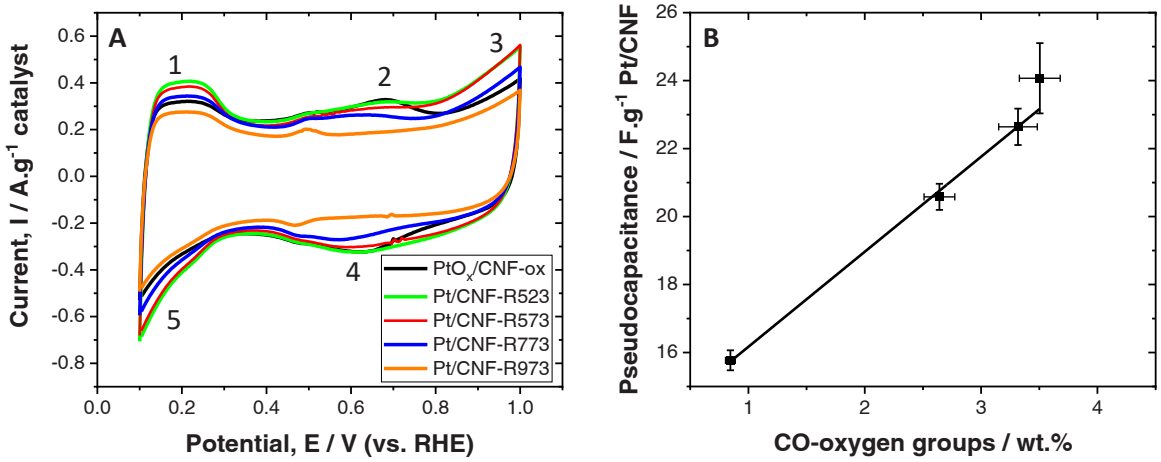

Fig. 1. A) Cyclic voltammograms of Pt/CNF catalysts in 0.1 M H_2SO_4 at a scan rate of 5 mV.s^{-1} and B) the relation between the pseudocapacitance of the Pt/CNF catalysts derived from CV as a function of the content of CO-oxygen groups (phenols and carbonyls/quinones) determine by TGA ($R^2 = 0.99$).

and carbonyl/quinone groups on the catalyst support. The successive heat treatment step, going from Pt/CNF-R523 to Pt/CNF-R973, results in a gradual decrease of peaks 2 and peak 4. This shows the gradual removal of lactone, phenol and carbonyl/quinone groups from the support as a result of increasing treatment temperature. The charge related to the oxidation of these support oxygen groups [55,70] is also known as the pseudocapacitance and can increase the specific capacitance (*e.g.*, pseudocapacitance plus double layer charging) of the Pt/CNF catalysts [51,71].

It has been shown before that the specific capacitance is related to the content of phenol and carbonyl/quinone groups present on the support [51,71]. To study this relation the specific capacitance was derived from the currents measured at peak 2 (0.4–0.8 V *vs.* RHE) from the anodic scan[14] [54], was plotted as a function of the content of lactone, phenol and carbonyl/quinone support groups (thermogravimetrically measured oxygen groups decomposed above 673 K, given in Table 1) in Fig. 1B [71]. This graph shows a linear correlation between the specific capacitance and the number of oxygen groups that decompose above 673 K (lactone, phenol and carbonyl/quinone groups), confirming the presence of these support oxygen groups under electrochemical conditions.

3.2. Characterization of platinum supported on carbon nanofiber catalysts

In addition to the change in CV features related to the content of oxygen groups on the carbon support, also a change in CV features related to Pt on the carbon support can be observed (Fig. 1A, peaks 1, 3 and 5). After the first reduction step, going from PtO$_x$/CNF-ox to Pt/CNF-R523, an increase in these peaks can be observed. This indicates that for Pt/CNF-R523 there is a larger exposed Pt surface area available for hydrogen adsorption/desorption or that the PtO$_x$/CNF-ox bears a certain amount of electrochemically inactive Pt which is still partially oxidized (Fig. S8) and therefore exposes fewer metallic Pt sites for hydrogen adsorption/desorption, even after several oxidative and reductive cycles. A similar low uptake for a low-temperature reduced Pt/CNF was found by Toebes et al. and low-temperature heat-treated Pt/CNT was found by Jiang et al.[66,72] The difference in Pt oxidation state between PtO$_x$/CNF-ox and Pt/CNF-R523 makes it impossible to relate changes in support oxygens between these two catalysts to a change in catalyst performance. Therefore, PtO$_x$/CNF-ox has been omitted from further discussions.

In Fig. 1A it can also be observed that an increase in heat treatment temperature, going from Pt/CNF-R523 to Pt/CNF-R973, results in a decrease of peaks 1, 3 and 5. The decrease in these peaks suggests that the exposed Pt surface area gradually decreases with increasing heat treatment temperature [72,73]. This can be explained by sintering of Pt particles at elevated temperatures, thereby increasing the average Pt particle size [73], as will be discussed now (Table 2).

Table 2 shows the metal loading determined by TGA, the ECSA of the synthesized catalysts determined by CO-stripping, and the average Pt particle size derived from the ECSA and HAADF-STEM [56].

The metal loading of the catalysts was determined by TGA using combustion up to 1173 K. For all the catalysts the metal loading was found to be between 5.2 and 5.6 wt%, thus showing that the metal loading is consistent.

The ECSA of the catalysts were calculated from CO-stripping curves, as will be discussed later (*vide infra*, Fig. 4), assuming a charge of 420 mC.cm^{-2} for the oxidation of a monolayer of linearly adsorbed CO [74]. With an increase in heat treatment, going from Pt/CNF-R523 to Pt/CNF-R973, the ECSA decreases gradually from 215 to 138 cm^2 Pt.g^{-1} Pt/CNF, corresponding to an increase in average Pt particle size from 1.5 to 2.3 nm [73]. These results coincide with the observations made for the decrease in hydrogen adsorption/desorption and platinum oxidation peaks (Fig. 1A).

The surface area average Pt particle size derived from HAADF-STEM images shows an increase in surface area average Pt particle size for Pt/CNF-R523 from 1.7 nm to 2.3 nm for the sample heat-treated at 973 K. The surface area average Pt particle size determined by HAADF-STEM matches well with the ECSA derived by CO-stripping. This shows that the Pt/CNF catalysts were well wetted, otherwise the values from Pt particle size derived from ECSA should have been significantly larger

Table 2
The Pt load, the surface area average Pt particle size based on HAADF-STEM imaging, the average Pt particle size derived from the ECSA, and the ECSA of the synthesized Pt/CNF catalysts.

	TGA	CO-stripping		HAADF-STEM
Catalyst	Pt loading (wt%)	Pt surface area (cm^2 Pt.g^{-1} Pt/CNF)	Pt particle size (nm)[a]	Surface based Pt particle size (nm)
Pt/CNF-R523	5.5	215 ± 4	1.5	1.7
Pt/CNF-R573	5.6	219 ± 2	1.5	-
Pt/CNF-R773	5.2	187 ± 2	1.7	2.2
Pt/CNF-R973	5.4	138 ± 6	2.3	2.3

[a] The average Pt particle size was calculated from the ECSA based on the relation $d = 6 \times 10^3$ / (ECSA x ρ), where ρ is the density of Pt (21.45 g/cm^3).

than from HAADF-STEM.

HAADF-STEM images were analyzed to evaluate the surface area average and number average Pt particle sizes including Pt particles < 1.5 nm. The HAADF-STEM images (Fig. 2A and Fig. S9A-B) reveal that the Pt particles are homogeneously distributed over the carbon nanofiber support. The number average Pt particle size distribution in Fig. 2B shows a log-normal distribution for the Pt particle with a size range between 0.5 and 3 nm and a few particles > 3.5 nm. With increasing heat treatment temperature, a shift in the log-normal distribution towards larger Pt particles can be observed, caused by sintering of Pt [75].

Besides the ECSA, CO-stripping was performed to determine the surface properties of the different Pt/CNF electrocatalysts. The background corrected CO-stripping curves are given in Fig. 3 [57].

The CO-stripping curves in Fig. 3 show for all the catalysts one main peak around 0.8 V, while for Pt/CNF-R973 there is also a preceding plateau between 0.4 V and 0.7. This plateau is related to CO oxidation at surface defects (kinks and step sites) [76,77], indicative that the high temperatures to which Pt/CNF-R973 has been exposed resulted in some surface defects on the Pt surface. The main peak is by far the main contributor to CO oxidation and appears to compose of a single peak, which indicates that the Pt nanoparticles of all the catalysts have a similar surface structure [76–78].

Fig. 4 displays the *in situ* HERFD-XANES spectra of Pt/CNF-R523, Pt/CNF-R773, and Pt/CNF-R973 recorded at 0.4 V *vs.* RHE in 0.1 M H_2SO_4. All XANES spectra show similar features and Pt/CNF-R523 will be discussed in detail as a representative example. The spectrum of Pt/CNF-R523 shows the main adsorption peak (the whiteline) at 11564.5 eV, which is typical for Pt [79]. The absorption intensity increases from 2.23 to 2.48 when stepping the electrode (Fig. S10A) from 0.1 to 0.78 V *vs.* RHE. This corresponds to an increase in unoccupied d-character states of the Pt catalyst and can be related to the adsorbed species on Pt at various potentials [79–81]. At 0.1 V *vs.* RHE, Pt is covered with *H, which causes antibonding states, yielding a broadened and lowered whiteline [79]. As the potential is increased to 0.4 V *vs.* RHE, this *H is replaced by *OH adsorbed at the top of Pt step edges and corners [79,80]. With a further increase in potential to 0.64 V and 0.78 V *vs.* RHE, the surface coverage of *OH increases through adsorption at the bottom of step edges and concave sites, thereby increasing absorption [79,81]. Thus, the replacement of *H with *OH and the successive gradual increase in *OH coverage increases the number of unoccupied d-states of the Pt catalyst.

For the different Pt/CNF catalysts, the whiteline gives a similar trend (Fig. 4A), as a function of the applied potential (Fig. S10A-C), and therefore shows a similar oxidation state. The similarity in the Pt oxidation state on the CNF support functionalized with various amounts of support oxygen groups and different Pt particle sizes are in accordance with XPS Pt_{4f} scan (Fig. S11 and Table S4). This similarity in the

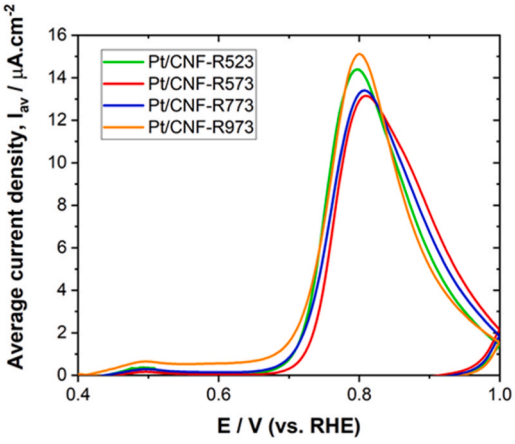

Fig. 3. Background corrected CO-stripping curves corrected for of Pt/CNF catalysts obtained in 0.1 M H_2SO_4 recorded at 5 mV.s^{-1}.

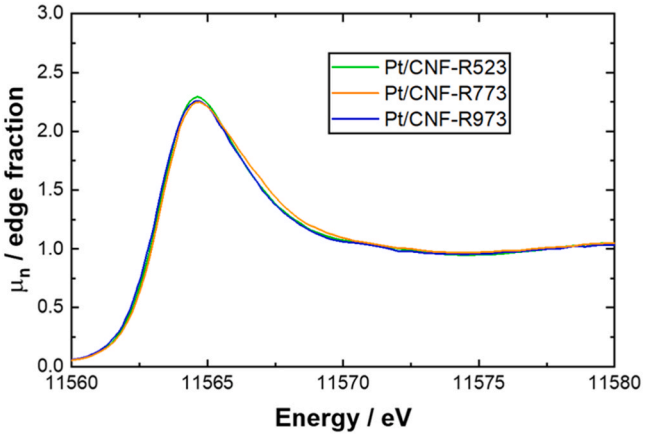

Fig. 4. Pt L_{III}-edge HERFD-XANES spectra of Pt/CNF catalysts measured in 0.1 M H_2SO_4 at 0.4 V *vs.* RHE hold potential.

Pt oxidation state for the different Pt/CNF catalysts indicates that the electronic property of Pt is not significantly affected by the Pt particle size or by the presence of lactone, phenol and carbonyl/quinone support oxygen groups, which is in line with thermocatalytic research [66,69].

Moreover, Pt/CNF-R523 has a significant amount of reduced support oxygen groups (hydroxyls) at 0.4 V *vs.* RHE and oxidized support oxygen groups (carbonyls) at 0.78 V *vs.* RHE present on the support (discussed

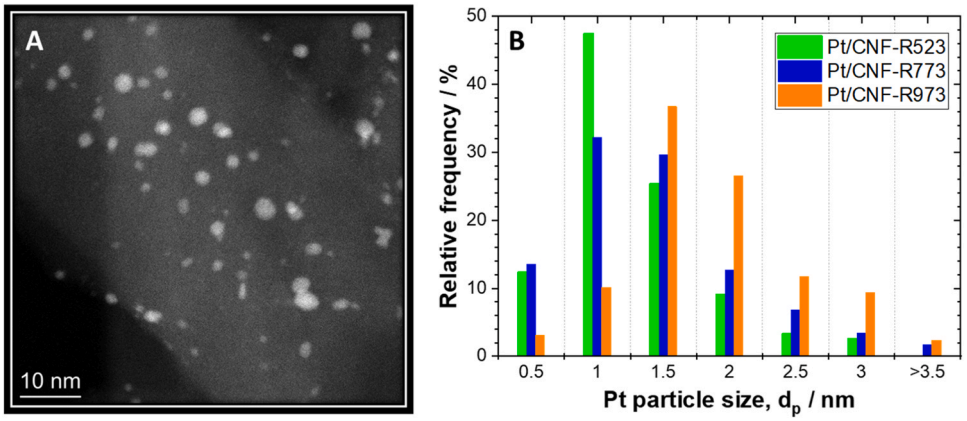

Fig. 2. A) HAADF-STEM images of Pt/CNF-R523 and B) the relative frequency of the number average Pt particle size measured on the CNF supports for various catalysts.

in Fig. 2A), while Pt/CNF-R973 bears hardly any support oxygen groups. Therefore, the agreement between the Pt spectral shapes of those two catalysts recorded at 0.4 V *vs.* RHE and 0.78 V *vs.* RHE, as well as the close resemblance of their corresponding Δμ spectra (S10G and S10I) indicates that the electronic structure of the electrochemically accessible Pt species is not affected by the oxidized nor the reduced state of the lactone, phenol and carbonyl/quinone oxygen groups present on the support.

3.3. Electrocatalytic oxidation of glucose

The four different Pt/CNF catalysts were tested for their activity toward the electrocatalytic oxidation of glucose. Linear sweep voltammetries of a bare CNF support in the absence and presence of glucose can be found in Fig. S12, which shows that bare CNF is inactive for catalyzing glucose oxidation reactions. The catalyst activity for the electrocatalytic oxidation of glucose was studied by background-corrected linear sweep voltammetry in 0.1 M H_2SO_4 (Fig. 5A). The background-corrected linear sweep voltammetries were derived from the linear sweep voltammetries in the presence and absence of glucose (Fig. S13).

The linear sweeps of the different Pt/CNF catalysts show three oxidation peaks at 0.45 V (peak 1), 0.62 V (peak 2) 0.78 V (peak 3). Peak 1 is related to dehydrogenative adsorption of glucose at the anomeric carbon (RCHOH → $R\dot{C}OH_{ads}Pt + H^+ + e^-$) as was shown for alkaline and acidic media [82–84]. Peaks 2 and 3 have been attributed to the electrocatalytic oxidation of glucose oxidation products [85], which can either be the oxidation of the adsorbed glucose to an adsorbed gluconolactone ($R\dot{C}OH_{ads}Pt \rightarrow R\dot{C}{=}O_{ads}Pt$) [86] or the oxidation of gluconolactone itself [84]. Alternatively, these two peaks also suggest that there are glucose oxidation products weakly (peak 2) and strongly (peak 3) adsorbed to the Pt surface, which is indicative of the presence of different Pt facets [85,87,88].

From the linear sweep voltammetries and up to 0.5 V it can be observed that the current densities are similar for all catalysts. This indicates that the catalyst activity is similar for all the catalysts up to this point and that the catalyst activity towards glucose dehydrogenation is not affected by the difference in catalyst properties. Above 0.5 V and up to 0.9 V, going from Pt/CNF-R523 to Pt/CNF-R973, a gradual decrease in current density is observed. This points to a decrease in catalytic activity for catalysts that have been exposed to higher heat treatment temperatures.

To evaluate whether the change in catalytic activity does not originate from diffusion limitation a similar experiment was performed, but then under convection with increased glucose concentration (Fig. S14). Under these reaction conditions, the current density went up by the same order of magnitude (2.7 and 3.5-fold for Pt/CNF-R523 and Pt/CNF-R973 respectively), which indicates that both systems suffer from similar extents of diffusion limitations which thus still allows us to compare catalytic activities.

To evaluate where the difference in catalytic activity originates from, the peak current densities measured by LSV at 0.78 V (I_p, Fig. 5B) have been plotted against the specific capacitance and the average Pt particle diameter (derived from the ECSA) of the Pt/CNF catalysts. Both the Pt particle size and the specific capacitance show a linear correlation with the peak current density. This indicates that both changes in catalyst properties might affect the catalyst activity. However, a change in ECSA-normalized catalytic activity induced by a difference in particle size would require a difference in electronic properties of the Pt particles or a difference in Pt surface structure for the different Pt/CNF catalysts. Yet, a difference in electronic properties was not found by *in-situ* HERFD-XANES (Fig. 4) and Pt_{4f} XPS (Fig. S11 and Table S4), nor was a difference in Pt surface structure found by CO-stripping (Fig. 3). Therefore, a change in catalytic activity should be related to a change in specific capacitance which in turn influences reactant/product adsorption. Since the specific capacitance is strongly related to the lactone, phenol, and carbonyl/quinone groups present on the support (Fig. 1B) [51,71], we argue that the presence of these support oxygen groups influences the catalytic performance. The fact that this increase in activity can only be seen at $E \geq 0.5$ V *vs.* RHE might originate from the nature of the support oxygen groups, namely, at $E \geq 0.5$ V *vs.* RHE (determined by CV, Fig. 1A) the support oxygen groups are oxidized to C═O groups [70]. These C═O groups could promote the formation of hydrogen bridges with the C-H and C-OH groups of glucose and thereby improve the adsorption of glucose in the annulus of the Pt nanoparticles, consequently increasing the catalyst activity. Therefore, we argue that the enhanced adsorption of glucose mediated by oxidized support oxygen groups increases the number of glucose molecules in vicinity of the Pt catalysts and thereby improves the catalyst activity.

Chronoamperometry was performed at 0.78 V *vs.* RHE to evaluate whether the difference in catalytic activity observed by LSV is not a temporary effect but also remains during longer reaction times (Fig. 6A) and to gain initial insights on the catalyst selectivity. Regarding the catalyst selectivity, preliminary results indicate that all catalysts predominantly form gluconic acid (>80%) [89]. After 30 min and going from Pt/CNF-R523 to Pt/CNF-R973, a gradual decrease in current density can be observed. This decrease in current density shows that

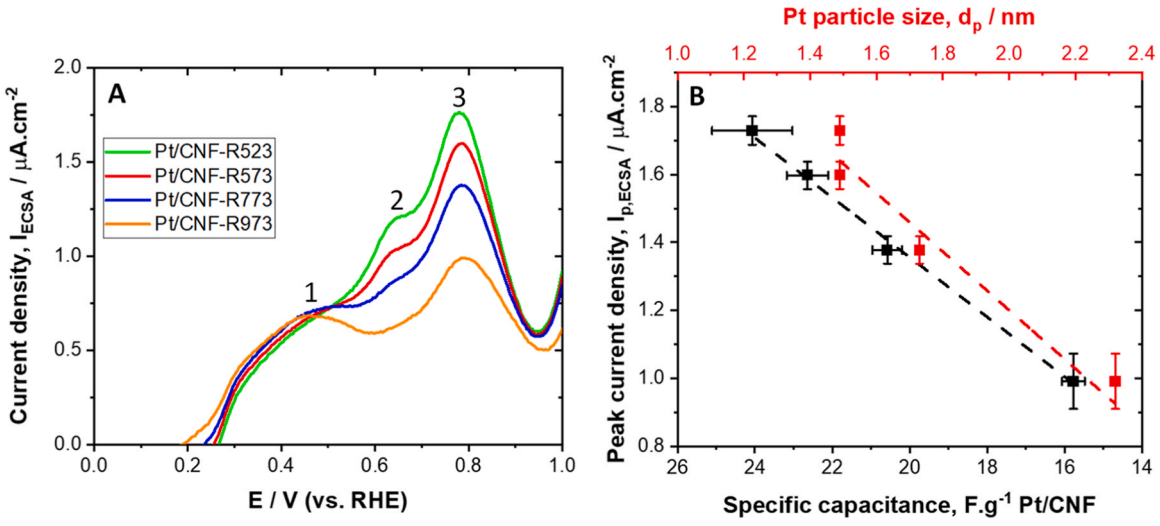

Fig. 5. A) Background corrected linear sweep voltammetry measured in 0.1 M H_2SO_4 in the presence of 0.1 M glucose at 1 mV.s^{-1} and B) the corresponding peak current density measured by LSV at 0.78 V *vs.* RHE as a function of the specific capacitance ($R^2 = 0.99$) and Pt particle size ($R^2 = 0.90$) of the Pt/CNF electrocatalysts.

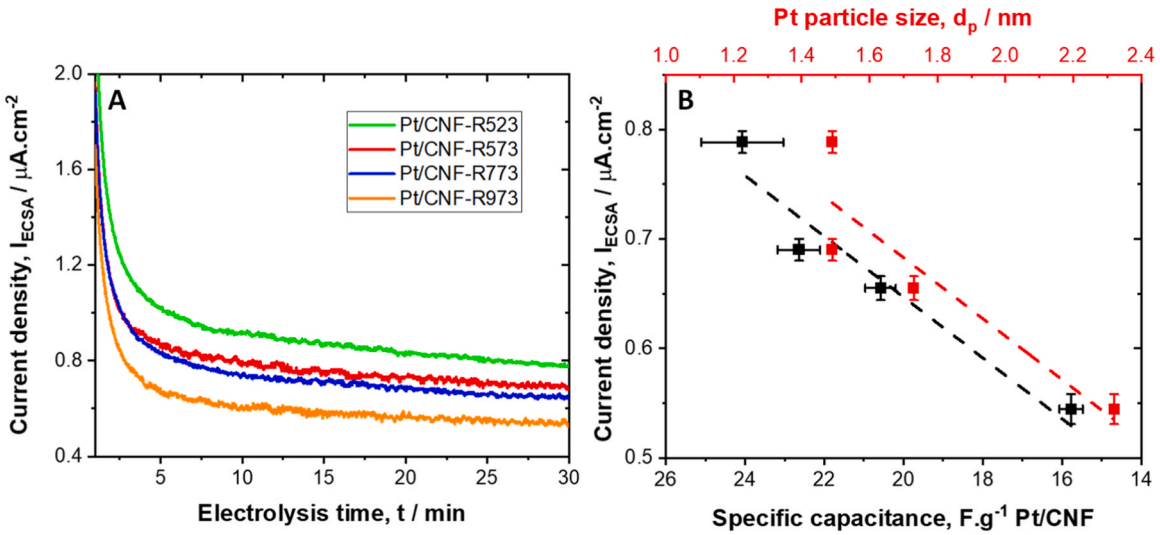

Fig. 6. A) Background-corrected current densities measured in 0.1 M H_2SO_4 in the presence of 0.1 M glucose at 0.78 V *vs.* RHE and B) the corresponding current density measured after 30 min chronoamperometry as a function of the specific capacitance (R^2 = 0.91) and Pt particle size (R^2 = 0.76) of the Pt/CNF electrocatalysts.

catalysts exposed to higher heat treatment temperatures have lower catalytic activity, confirming the results made by LSV. Moreover, this difference in current densities after 30 min of CA shows that the variance in catalytic activity is not a temporary effect.

The current densities measured after 30 min CA have been plotted against the specific capacitance and the Pt particle size for the Pt/CNF catalysts in Fig. 6B to re-evaluate the origin of the difference in catalytic activity. Once again, the specific capacitance (*e.g.*, the content of lactone, phenol and carbonyl/quinone support oxygen groups) has a linear correlation with the catalyst activity, thereby confirming the results obtained by LSV.

The most accepted reaction mechanism requires both the adsorption of glucose and hydroxyls on the Pt surface before glucose can be catalytically oxidized by Pt. The ratio between different adsorbates can influence the catalyst activity. This adsorbate coverage can be estimated from the XANES spectra and the associated difference XANES spectra [64,90] by using LCA, which is based on Fig. S10A-L. The estimate of the relative coverages of each adsorbate for three different Pt/CNF catalysts is shown in Fig. 7A-C.

Fig. 7A compares the calculated intensity for each adsorbate component in the fitting results of a Pt/CNF-R523 catalyst as a function of potential. At 0.1 V *vs.* RHE and in the presence of 0.1 M glucose, the surface of Pt is free of adsorbed *OH and completely covered with adsorbed *glucose. This is a direct result of the methodology for estimating the coverage of species since the spectrum at 0.1 V *vs.* RHE in the presence of glucose corresponds to the base spectrum of Pt and the *glucose difference spectrum. As the potential is increased to 0.78 V *vs.* RHE, the content of adsorbed *glucose gradually decreases, while the content of *OH increases. This indicates that *OH adsorbates replace the adsorbed *glucose at higher potentials, which agrees with the results reported for the adsorbate coverage in ethanol oxidation of Pt electrodes [64,90]. A successive increase in potential to 1.0 V results in a loss of adsorbates due to the formation of a PtO_x species. Also, this is a direct result of the methodology for estimating the coverage of species, since the spectrum at 1.0 V *vs.* RHE in the presence of glucose corresponds to the base spectrum of Pt and PtO_x difference spectrum [64]. Here it is argued that the PtO_x species causes the desorption of adsorbates, resulting in a loss in catalytic activity of Pt in acidic media at pH 1, which coincides with a decrease in catalytic activity as was shown in Fig. 5A [91].

A similar trend of adsorbates as a function of potential for Pt/CNF-R523 can be observed for Pt/CNF-R773 and Pt/CNF-R973 (Fig. 7A-C), which indicates that the potential-dependent adsorbate coverage is similar between these Pt/CNF catalysts. Hence, the ratio between adsorbates present on the Pt surface for the Pt/CNF electrocatalysts is not affected by the content of lactone, phenol and carbonyl/quinone support oxygen groups. In other words, the steady state of the Pt surface is the same for all measured catalysts. Nonetheless, an increase in catalytic

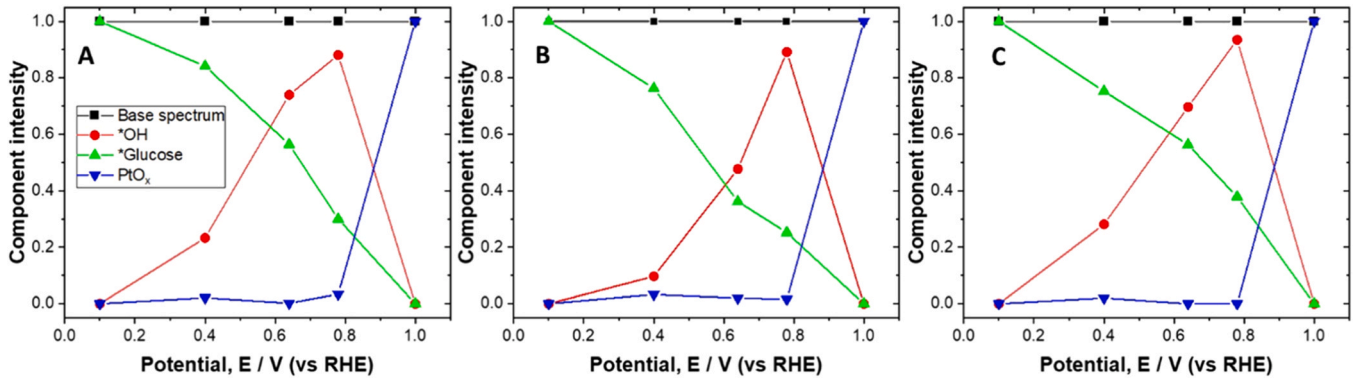

Fig. 7. Results of LCA of HERFD-XANES spectra at Pt L_{III}-edge obtained at various hold potentials in 0.1 M H_2SO_4 and 0.1 M glucose for Pt/CNF-R523 (A), Pt/CNF-773 (B) and Pt/CNF-R973 (C).

activity was observed for Pt/CNF catalysts with higher contents of lactone, phenol and carbonyl/quinone support oxygen groups (Figs. 5B and 6B). This indicates that the improved catalytic activity induced by support oxygen groups is likely to originate from improved glucose turnover. We suggest that this improvement stems from accelerated reactant adsorption in the annulus of the Pt particles, caused by the formation of hydrogen bridges between C═O support groups ($E \geq 0.5$ V *vs.* RHE) and C-H and C-OH groups of glucose. As a result, the content of reactive species increases in the annulus of the Pt particles. This hypothesis will be quantified in the following section, where electrochemically oxidized Pt/CNF-R523 and Pt/CNF-R973 will be used as a base case scenario.

Pt/CNF-R523, Pt/CNF-R773 and Pt/CNF-R973 were electrochemically oxidized to Pt/CNF-R523-EO, Pt/CNF-R773-EO and Pt/CNF-R973-EO to re-introduce support oxygen on the carbon support. On the one hand, CO-stripping (Fig. S15) showed that the electrochemical oxidization of the catalysts did not induce significant changes in the ECSA and resulted in catalysts with similar Pt surface structures. On the other hand, CV (Fig. S16) showed that the specific capacitance increased sufficiently to oxidize the carbon support in the annulus of the Pt particles.

The activity towards the electrooxidation of glucose was evaluated by LSV for Pt/CNF-R523, Pt/CNF-R773 and Pt/CNF-R973 before and after electrochemical oxidation (Fig. 8). After electrochemical oxidation, all three catalysts show a significant increase in current density above 0.5 V *vs.* RHE compared to their non-oxidized counterparts. At 0.78 V *vs.* RHE going from Pt/CNF-R523 to Pt/CNF-R523-EO, the current density increases from 1.8 to 3.0 $\mu A.cm^{-2}$, while the current density from Pt/CNF-R773 to Pt/CNF-R773-EO increases from 1.4 to 2.7 $\mu A.cm^{-2}$, and the current density from Pt/CNF-R973 to Pt/CNF-R973-EO increases from 1.0 $\mu A.cm^{-2}$ to 2.4 $\mu A.cm^{-2}$. For Pt/CNF-R523, Pt/CNF-R773 and Pt/CNF-R973, this increase in current density corresponds to an increase in catalytic activity of 72%, 93% and 144% respectively. This increase in catalytic activity after electrochemical oxidation of the Pt/CNF catalyst indicates that the introduction of support oxygen groups improves the catalyst activity. The increasing trend in catalytic activity (*e.g.*, 72–93–144%) induced by electrochemical oxidation can be attributed to the decreasing content in support oxygen groups before electrochemical oxidation, going from Pt/CNF-R973 to Pt/CNF-R523.

Table 3 gives an overview of the reaction conditions and the measured current densities for the electrocatalytic oxidation of glucose on Pt electrodes in acidic medium reported in this study and literature [89,92,93]. Considering the difference in scan rates, the current density reported in this study of Pt/CNF-R523-EO corresponds well with the current densities (*e.g.*, catalytic activity) reported in the literature.

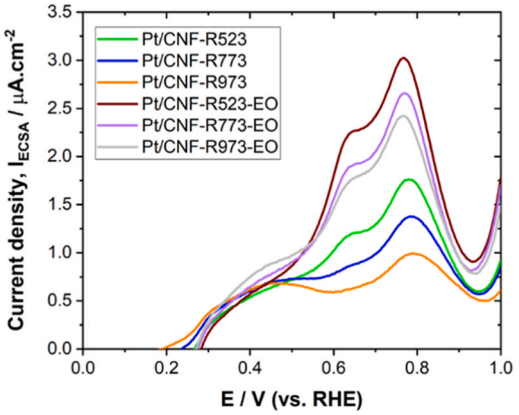

Fig. 8. Background corrected linear sweep voltammetry measured at 1 $mV.s^{-1}$ in 0.1 M H_2SO_4 and 0.1 M glucose for pristine Pt/CNF-R523, Pt/CNF-R773 and Pt/CNF-R973 and Pt/CNF-R523-EO, Pt/CNF-R773-EO and Pt/CNF-R973-EO.

Generally, the measured current is normalized by the active surface area of the supported metallic catalyst (ECSA), to compare the catalytic activity of two different catalysts. However, the presence of oxygen groups on the carbon support can facilitate the adsorption of reactants in the annulus of the Pt particles [19,69], which increases available species in proximity of the metal catalyst that are susceptible to conversion (Fig. 9A) and can thereby improve the catalyst activity. In line with this reasoning, the measured currents were normalized by both the active surface area of the metallic catalyst and the annulus around the perimeter of the catalyst nanoparticles (ASA = ECSA + annulus area). The surface area of the annulus can be calculated with the inner radius of the annulus (r) and the outer radius of the annulus (R), where r = Pt nanoparticle radius and R = Pt nanoparticle radius + length of glucopyranose (0.84 nm) (calculations in supporting information "Current normalization by adsorbable surface area"). Based on these considerations, the ASA changes with the radius of the Pt nanoparticles, where smaller Pt nanoparticles (Pt/CNF-R523-EO) are more influenced by the annulus surface area than larger Pt particles (Pt/CNF-R973-EO), illustrated in Fig. 9A.

Fig. 10 shows the background-corrected LSV at E = 0.5–1.0 V *vs.* RHE for the electrocatalytic oxidation of glucose over Pt/CNF-R523-EO, Pt/CNF-R773-EO and Pt/CNF-R973-EO and the related currents densities normalized by the ECSA (I_{ECSA}) and ASA (I_{ASA}), to evaluate how this affects the current densities. The I_{ECSA} is higher than the I_{ASA} for all catalysts since the ECSA is smaller than the ASA (Fig. 9). Going from Pt/CNF-R523-EO to Pt/CNF-R973-EO, the I_{ECSA} decreases, while the I_{ASA} is nearly identical for all catalysts. Moreover, the relative difference between I_{ECSA} and I_{ASA} decreases from Pt/CNF-R523-EO to Pt/CNF-R973-EO. The increasing difference between the I_{ECSA} and I_{ASA} when going from Pt/CNF-R523-EO to Pt/CNF-R973-EO can be explained by the larger contribution of the annulus for catalysts that bare smaller Pt particles. In this case, the Pt particles are 1.6, 1.8 and 2.2 nm for Pt/CNF-R523-EO, Pt/CNF-R773-EO and Pt/CNF-R973-EO respectively. More remarkable is that the current density based on ASA is nearly the same for all catalysts, indicative that the catalyst activity can best be described by the adsorbable surface area on the metal surface and in the annulus of the metal particles.

4. Conclusion

We observed that the heat treatment of Pt/CNF functionalized with support oxygen groups (*e.g.*, lactone, phenol and carbonyl/quinone groups) resulted in a gradual increase in Pt particle size and a gradual decrease in the content of support oxygen groups. As a result, catalysts were obtained with different Pt particle sizes and different contents of support oxygen groups. The difference in Pt particle size and content of support oxygen groups did not affect the Pt surface structure, the Pt electronic properties, and the ratio between adsorbates on the Pt surface during the electrocatalytic oxidation of glucose. Despite this, the catalytic activity evaluation showed a direct correlation between the activity and the support oxygen group content. More specifically, the introduction of support oxidation groups in the annulus of the Pt particles by electrochemical oxidation resulted in an approximately 2.5-fold increase in catalytic activity. This increase in catalytic activity was found to be higher for electrochemically oxidized Pt/CNF functionalized with smaller Pt particles. In this case, we argue that the annulus for smaller Pt particles plays a more significant role in the adsorption of reactants in the vicinity of the Pt catalyst. Therefore, we conclude that support oxygen groups improve the adsorption of reactants in vicinity of the Pt catalyst and thereby improve the catalyst activity.

CRediT authorship contribution statement

M.P.J.M. van der Ham: Contributed to the investigation, Validation, Conceptualization, Formal analysis, Writing – original draft, Data curation of the research. **T.J.P. Hersbach:** Contributed to investigation

Table 3
Summary of current densities reported in the literature for the electrocatalytic oxidation of glucose on Pt in acidic medium.

Catalyst	Technique	Electrolyte	Glucose concentration M	Scan rate $mV.s^{-1}$	Current density $\mu A.cm^{-2}$	Reference
Pt/CNF-R523-EO	LSV	0.1 M H2SO4	0.1	1	3	This work
Pt/C	CV	0.1 M HClO4	0.1	20	18	[92]
Pt	CV	0.1 M HClO4	0.1	50	55	[93]
Pt	CV	0.1 M HClO4	0.2	50	55	[89]

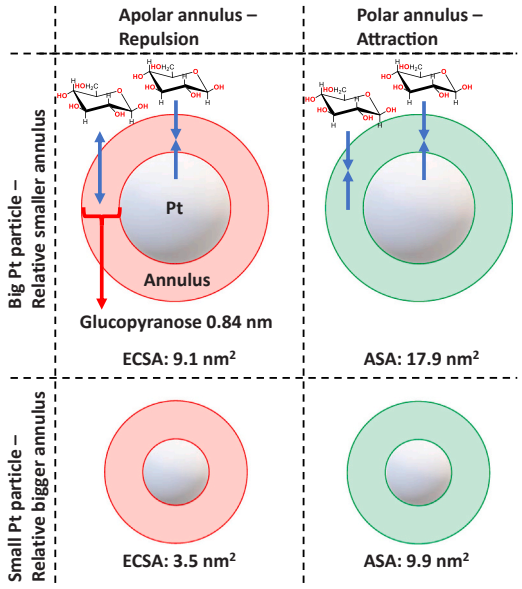

Fig. 9. Top view of a small (1.5 nm) and (2.4 nm) big Pt particle on a carbon support. The annulus of the Pt particle is either non-functionalized (red) or functionalized with support oxygen groups (green), resulting in the repulsion or adsorption of a substrate (*e.g.* glucopyranose) respectively. The electrochemical active surface area (ECSA) of the Pt particles are given in grey, while the adsorbable surface area (ASA) of glucopyranose is given in grey and green.

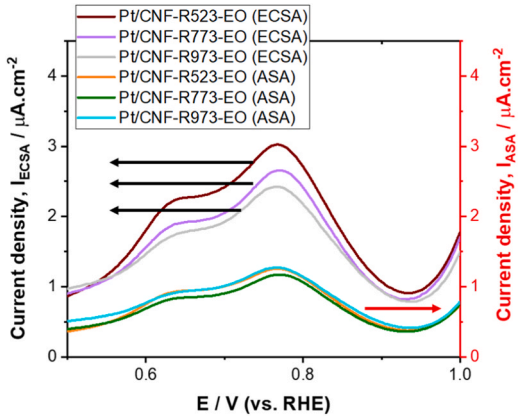

Fig. 10. Background-corrected linear sweep voltammetry measured at 1 mV. s^{-1} in 0.1 M H_2SO_4 and 0.1 M glucose, with currents normalized by the ECSA and ASA for Pt/CNF-R523-EO, Pt/CNF-R773-EO and Pt/CNF-R973-EO.

and formal analysis, more specifically XANES data collection and analysis and, and Writing – review & editing. **J.J. Delgado:** Contributed to investigation and formal analysis, more specifically HAADF-STEM data collection and analysis. **B.D. Matson:** Contributed to investigation, more specifically XANES data collection. **J. Lim:** Contributed to investigation, more specifically XANES data collection. **M. Führer:** Contributed to the methodology, more specifically on how to synthesize CNF and impregnate them with Pt. T. van Haasterecht: Contributed to formal analysis, more specifically XRD and XPS data collection and analysis. **M. W.G.M. Verhoeven:** Contributed to investigation and formal analysis, more specifically XPS data collection and analysis. E.J.M. Hensen: Contributed to validation of XPS data analysis and collection and, Writing – review & editing. **D. Sokaras:** Contributed to investigation and formal analysis, more specifically XANES data collection and analysis. **M.T.M. Koper:** Contributed to supervision and Writing – review & editing. **J.H. Bitter:** Contributed to supervision, Funding acquisition, Writing – review & editing and Visualization.

Declaration of Competing Interest

The authors declare that they have no known competing financial interests or personal relationships that could have appeared to influence the work reported in this paper.

Data availability

Data will be made available on request.

Acknowledgments

This work is part of the research program Electrons to Chemical Bonds (E2CB) with project number P17–08-05 and is partially financed by the Dutch Research Council (NWO). Use of the Stanford Synchrotron Radiation Lightsource, SLAC National Accelerator Laboratory, was supported by the U.S. Department of Energy, Office of Science, Office of Basic Energy Sciences under Contract No. DE-AC02–76SF00515. This research used resources of the National Energy Research Scientific Computing Center (NERSC), a U.S. Department of Energy Office of Science User Facility operated under Contract No. DE-AC02–05CH11231. The HAADF-STEM measurements were financed by MINECO (Spain) and Junta de Andalucia through projects PID2020–113809RB-C33 and PY18–2727.

Appendix A. Supporting information

Supplementary data associated with this article can be found in the online version at doi:10.1016/j.apcatb.2023.123046.

References

[1] E. Derrien, M. Mounguengui-Diallo, N. Perret, P. Marion, C. Pinel, M. Besson, Aerobic oxidation of glucose to glucaric acid under alkaline-free conditions: Au-based bimetallic catalysts and the effect of residues in a hemicellulose hydrolysate, Ind. Eng. Chem. Res. 56 (2017) 13175–13189, https://doi.org/10.1021/acs.iecr.7b01571.

[2] D. Bin, H. Wang, J. Li, H. Wang, Z. Yin, J. Kang, B. He, Z. Li, Controllable oxidation of glucose to gluconic acid and glucaric acid using an electrocatalytic reactor, Electro Acta 130 (2014) 170–178, https://doi.org/10.1016/j.electacta.2014.02.128.

[3] S. Verma, S. Lu, P.J.A. Kenis, Co-electrolysis of CO_2 and glycerol as a pathway to carbon chemicals with improved technoeconomics due to low electricity consumption, Nat. Energy 4 (2019) 466–474, https://doi.org/10.1038/s41560-019-0374-6.

[4] W.J. Liu, Z. Xu, D. Zhao, X.Q. Pan, H.C. Li, X. Hu, Z.Y. Fan, W.K. Wang, G.H. Zhao, S. Jin, G.W. Huber, H.Q. Yu, Efficient electrochemical production of glucaric acid and H2 via glucose electrolysis, Nat. Commun. 11 (2020) 1–11, https://doi.org/10.1038/s41467-019-14157-3.

[5] T. Rafaïdeen, S. Baranton, C. Coutanceau, Highly efficient and selective electrooxidation of glucose and xylose in alkaline medium at carbon supported alloyed PdAu nanocatalysts, Appl. Catal. B 243 (2019) 641–656, https://doi.org/10.1016/j.apcatb.2018.11.006.

[6] D. Zheng, J. Li, S. Ci, P. Cai, Y. Ding, M. Zhang, Z. Wen, Three-birds-with-one-stone electrolysis for energy-efficiency production of gluconate and hydrogen, Appl. Catal. B 277 (2020), https://doi.org/10.1016/j.apcatb.2020.119178.

[7] B.E. Hayden, D. Pletcher, J.-P. Suchsland, Enhanced activity for electrocatalytic oxidation of carbon monoxide on titania-supported gold nanoparticles, Angew. Chem. 119 (2007) 3600–3602, https://doi.org/10.1002/ange.200604633.

[8] J.R. Barbosa, M.N. Leon, C.M. Fernandes, R.M. Antoniassi, O.C. Alves, E.A. Ponzio, J.C.M. Silva, PtSnO2/C and Pt/C with preferential (100) orientation: High active electrocatalysts for ammonia electro-oxidation reaction, Appl. Catal. B 264 (2020), 118458, https://doi.org/10.1016/j.apcatb.2019.118458.

[9] A.C. Garcia, Y.Y. Birdja, G. Tremiliosi-Filho, M.T.M. Koper, Glycerol electro-oxidation on bismuth-modified platinum single crystals, J. Catal. 346 (2017) 117–124, https://doi.org/10.1016/j.jcat.2016.12.013.

[10] Q. Fu, X. Bao, Confined microenvironment for catalysis control, Nat. Catal. 2 (2019) 834–836, https://doi.org/10.1038/S41929-019-0354-Z.

[11] Y. Kwon, M.T.M. Koper, Electrocatalytic hydrogenation and deoxygenation of glucose on solid metal electrodes, ChemSusChem 6 (2013) 455–462, https://doi.org/10.1002/cssc.201200722.

[12] W. Feng, T. Wang, Q. Cui, Y. Yue, P. Yuan, Y. Cao, X. Bao, Impacts of support properties on the vacuum residue slurry-phase hydrocracking performance of Mo catalysts, SSRN Electron. J. (2022) 1–30, https://doi.org/10.2139/ssrn.3983894.

[13] M. Kourtelesis, T.S. Moraes, L.V. Mattos, D.K. Niakolas, F.B. Noronha, X. Verykios, The effects of support morphology on the performance of Pt/CeO2 catalysts for the low temperature steam reforming of ethanol, Appl. Catal. B 284 (2021), https://doi.org/10.1016/j.apcatb.2020.119757.

[14] J. Audevard, A. Benyounes, R. Castro Contreras, H. Abou Oualid, M. Kacimi, P. Serp, Multifunctional catalytic properties of Pd/CNT catalysts for 4-nitrophenol reduction, ChemCatChem 202101783 (2022), https://doi.org/10.1002/cctc.202101783.

[15] J. Chen, Z. Wu, H. Liu, X. Bao, P. Yuan, A surface-cofunctionalized silica supported palladium catalyst for selective hydrogenation of nitrile butadiene rubber with enhanced catalytic activity and recycling performance, Ind. Eng. Chem. Res 58 (2019) 11821–11830, https://doi.org/10.1021/acs.iecr.9b01468.

[16] I.C. Gerber, P. Serp, A theory/experience description of support effects in carbon-supported catalysts, Chem. Rev. 120 (2020) 1250–1349, https://doi.org/10.1021/acs.chemrev.9b00209.

[17] M.L. Toebes, F.F. Prinsloo, J.H. Bitter, A.J. Van Dillen, K.P. De Jong, Influence of oxygen-containing surface groups on the activity and selectivity of carbon nanofiber-supported ruthenium catalysts in the hydrogenation of cinnamaldehyde, J. Catal. 214 (2003) 78–87, https://doi.org/10.1016/S0021-9517(02)00081-7.

[18] A.J. Plomp, H. Vuori, A.O.I. Krause, K.P. de Jong, J.H. Bitter, Particle size effects for carbon nanofiber supported platinum and ruthenium catalysts for the selective hydrogenation of cinnamaldehyde, Appl. Catal. A Gen. 351 (2008) 9–15, https://doi.org/10.1016/j.apcata.2008.08.018.

[19] R.W. Gosselink, W. Xia, M. Muhler, K.P. De Jong, J.H. Bitter, Enhancing the activity of Pd on carbon nanofibers for deoxygenation of amphiphilic fatty acid molecules through support polarity, ACS Catal. 3 (2013) 2397–2402, https://doi.org/10.1021/cs400478q.

[20] P. Makowski, R. Demir Cakan, M. Antonietti, F. Goettmann, M.M. Titirici, Selective partial hydrogenation of hydroxy aromatic derivatives with palladium nanoparticles supported on hydrophilic carbon, Chem. Commun. (2008) 999–1001, https://doi.org/10.1039/b717928f.

[21] Z. Dong, A. Mukhtar, T. Ludwig, S.A. Akhade, S.Y. Kang, B. Wood, K. Grubel, M. Engelhard, T. Autrey, H. Lin, Efficient Pd on carbon catalyst for ammonium formate dehydrogenation: Effect of surface oxygen functional groups, Appl. Catal. B 321 (2023), https://doi.org/10.1016/j.apcatb.2022.122015.

[22] W. Shi, B. Zhang, Y. Lin, Q. Wang, Q. Zhang, D.S. Su, Enhanced chemoselective hydrogenation through tuning the interaction between pt nanoparticles and carbon supports: Insights from identical location transmission electron microscopy and x-ray photoelectron spectroscopy, ACS Catal. 6 (2016) 7844–7854, https://doi.org/10.1021/acscatal.6b02207.

[23] X. Ning, Y. Li, B. Dong, H. Wang, H. Yu, F. Peng, Y. Yang, Electron transfer dependent catalysis of Pt on N-doped carbon nanotubes: Effects of synthesis method on metal-support interaction, J. Catal. 348 (2017) 100–109, https://doi.org/10.1016/j.jcat.2017.02.011.

[24] R.C. Contreras, B. Guicheret, B.F. Machado, C. Rivera-Cárcamo, M.A. Curiel Alvarez, B. Valdez Salas, M. Ruttert, T. Placke, A. Favre Réguillon, L. Vanoye, C. de Bellefon, R. Philippe, P. Serp, Effect of mesoporous carbon support nature and pretreatments on palladium loading, dispersion and apparent catalytic activity in hydrogenation of myrcene, J. Catal. 372 (2019) 226–244, https://doi.org/10.1016/j.jcat.2019.02.034.

[25] S. Van De Vyver, J. Geboers, W. Schutyser, M. Dusselier, P. Eloy, E. Dornez, J. W. Seo, C.M. Courtin, E.M. Gaigneaux, P.A. Jacobs, B.F. Sels, Tuning the acid/metal balance of carbon nanofiber-supported nickel catalysts for hydrolytic hydrogenation of cellulose, ChemSusChem 5 (2012) 1549–1558, https://doi.org/10.1002/cssc.201100782.

[26] J. Dai, H. Zou, Z. Shi, H. Yang, R. Wang, Z. Zhang, S. Qiu, Janus N-Doped Carbon@Silica Hollow Spheres as Multifunctional Amphiphilic Nanoreactors for Base-Free Aerobic Oxidation of Alcohols in Water, ACS Appl. Mater. Interfaces 10 (2018) 33474–33483, https://doi.org/10.1021/acsami.8b11888.

[27] H. Markus, P. Mäki-Arvela, N. Kumar, N.V. Kul'kova, P. Eklund, R. Sjöholm, B. Holmbom, T. Salmi, D.Y. Murzin, Hydrogenolysis of hydroxymatairesinol over carbon-supported palladium catalysts, Catal. Lett. 103 (2005) 125–131, https://doi.org/10.1007/s10562-005-6514-6.

[28] A.C. Ghogia, B.F. Machado, S. Cayez, A. Nzihou, P. Serp, K. Soulantica, D. Pham Minh, Beyond confinement effects in Fischer-Tropsch Co/CNT catalysts, J. Catal. 397 (2021) 156–171, https://doi.org/10.1016/j.jcat.2021.03.027.

[29] B. Li, D. Su, The nucleophilicity of the oxygen functional groups on carbon materials: a DFT analysis, Chem. - A Eur. J. 20 (2014) 7890–7894, https://doi.org/10.1002/chem.201400347.

[30] X. Han, C. Li, Y. Guo, X. Liu, Y. Zhang, Y. Wang, N-doped carbon supported Pt catalyst for base-free oxidation of 5-hydroxymethylfurfural to 2,5-furandicarboxylic acid, Appl. Catal. A Gen. 526 (2016) 1–8, https://doi.org/10.1016/j.apcata.2016.07.011.

[31] Y. Peng, B. Lu, N. Wang, L. Li, S. Chen, Impacts of interfacial charge transfer on nanoparticle electrocatalytic activity towards oxygen reduction, Phys. Chem. Chem. Phys. 19 (2017) 9336–9348, https://doi.org/10.1039/c6cp08925a.

[32] H. Gharibi, F. Yasi, M. Kazemeini, A. Heydari, F. Golmohammadi, Fabrication of MEA based on sulfonic acid functionalized carbon supported platinum nanoparticles for oxygen reduction reaction in PEMFCs, RSC Adv. 5 (2015) 85775–85784, https://doi.org/10.1039/c5ra09201a.

[33] H.P. Yang, Q. Lin, H.W. Zhang, G.D. Li, L.D. Fan, X.Y. Chai, Q.L. Zhang, J.H. Liu, C. X. He, Platinum/nitrogen-doped carbon/carbon cloth: a bifunctional catalyst for the electrochemical reduction and carboxylation of CO_2 with excellent efficiency, Chem. Commun. 54 (2018) 4108–4111, https://doi.org/10.1039/c8cc00969d.

[34] Z.B. Wang, G.P. Yin, P.F. Shi, Effects of ozone treatment of carbon support on Pt-Ru/C catalysts performance for direct methanol fuel cell, Carbon N. Y 44 (2006) 133–140, https://doi.org/10.1016/j.carbon.2005.06.043.

[35] J.R.C. Salgado, R.G. Duarte, L.M. Ilharco, A.M. Botelho do Rego, A.M. Ferraria, M. G.S. Ferreira, Effect of functionalized carbon as Pt electrocatalyst support on the methanol oxidation reaction, Appl. Catal. B 102 (2011) 496–504, https://doi.org/10.1016/j.apcatb.2010.12.031.

[36] C. Alegre, M.E. Gálvez, E. Baquedano, E. Pastor, R. Moliner, M.J. Lázaro, Influence of support's oxygen functionalization on the activity of Pt/carbon xerogels catalysts for methanol electro-oxidation, : Int J. Hydrog. Energy, Pergamon (2012) 7180–7191, https://doi.org/10.1016/j.ijhydene.2011.11.022.

[37] N. Muthuswamy, J.L.G. De La Fuente, P. Ochal, R. Giri, S. Raaen, S. Sunde, M. Rønning, D. Chen, Towards a highly-efficient fuel-cell catalyst: Optimization of Pt particle size, supports and surface-oxygen group concentration, Phys. Chem. Chem. Phys. 15 (2013) 3803–3813, https://doi.org/10.1039/c3cp43659d.

[38] C. Alegre, M.E. Gálvez, E. Baquedano, R. Moliner, E. Pastor, M.J. Lázaro, Oxygen-functionalized highly mesoporous carbon xerogel based catalysts for direct methanol fuel cell anodes, J. Phys. Chem. C. 117 (2013) 13045–13058, https://doi.org/10.1021/jp400824n.

[39] D. Sebastián, M.J. Lázaro, R. Moliner, I. Suelves, A.S. Aricò, V. Baglio, Oxidized carbon nanofibers supporting PtRu nanoparticles for direct methanol fuel cells, : Int J. Hydrog. Energy, Pergamon (2014) 5414–5423, https://doi.org/10.1016/j.ijhydene.2013.12.005.

[40] A.J. Dillen, J.W. Geus, L.A.M. Hermans, J. Meijden, Production of supported copper and nickel catalysts by deposition-precipitation, Proc. 6th Int. Conf. Catal. 11 (1977) 677–685.

[41] K.P. De Jong, J.W. Geus, Carbon nanofibers: catalytic synthesis and applications, Catal. Rev. Sci. Eng. 42 (2000) 481–510, https://doi.org/10.1081/CR-100101954.

[42] J.H. Bitter, Dark material with a bright future: carbon as support in future heterogeneous catalysis – A short personal perspective, Catal. Today (2023), https://doi.org/10.1016/j.cattod.2023.01.022.

[43] M.C.O. Monteiro, M.T.M. Koper, Alumina contamination through polishing and its effect on hydrogen evolution on gold electrodes, Electro Acta 325 (2019), 134915, https://doi.org/10.1016/j.electacta.2019.134915.

[44] H.T. Fang, C.G. Liu, C. Liu, F. Li, M. Liu, H.M. Cheng, Purification of single-wall carbon nanotubes by electrochemical oxidation, Chem. Mater. 16 (2004) 5744–5750, https://doi.org/10.1021/cm035263h.

[45] Y. Yi, G. Weinberg, M. Prenzel, M. Greiner, S. Heumann, S. Becker, R. Schlögl, Electrochemical corrosion of a glassy carbon electrode, Catal. Today 295 (2017) 32–40, https://doi.org/10.1016/j.cattod.2017.07.013.

[46] Z. Kou, K. Cheng, H. Wu, R. Sun, B. Guo, S. Mu, Observable electrochemical oxidation of carbon promoted by platinum nanoparticles, ACS Appl. Mater. Interfaces 8 (2016) 3940–3947, https://doi.org/10.1021/acsami.5b11086.

[47] M.F. Lia, Q. Taoa, L.W. Liaoa, J. Xua, J. Caib, Y.X. Chena, Oxidation of carbon supports at fuel cell cathodes: differential electrochemical mass spectrometric study, Chin. J. Chem. Phys. 23 (2010) 442–446, https://doi.org/10.1088/1674-0068/23/04/442-446.

[48] M. Führer, T. van Haasterecht, J.H. Bitter, Cinnamaldehyde hydrogenation over carbon supported molybdenum and tungsten carbide catalysts, Chem. Commun. 58 (2022) 13608–13611, https://doi.org/10.1039/d2cc05322e.

[49] A.N. Salanov, N.M. Kochurova, A.N. Serkova, A.V. Kalinkin, L.A. Isupova, V. N. Parmon, Oxidation and recrystallization of platinum group metals (Pt, Pd, Rh) in oxygen. Surface and subsurface reconstruction of polycrystalline platinum during annealing in the O2 atmosphere over the temperature range of 600–1400 K, Appl. Surf. Sci. 490 (2019) 188–203, https://doi.org/10.1016/j.apsusc.2019.05.289.

[50] M. Göckeler, C.M. Berger, M. Purcel, R. Bergsträßer, A.P. Schinkel, M. Muhler, Surface reactions during temperature-programmed desorption and reduction experiments with oxygen-functionalized carbon blacks, Appl. Surf. Sci. 561 (2021), https://doi.org/10.1016/j.apsusc.2021.150044.

[51] A. Śliwak, B. Grzyb, J. Ćwikła, G. Gryglewicz, Influence of wet oxidation of herringbone carbon nanofibers on the pseudocapacitance effect, Carbon N. Y 64 (2013) 324–333, https://doi.org/10.1016/j.carbon.2013.07.082.

[52] M.C.O. Monteiro, F. Dattila, B. Hagedoorn, R. García-Muelas, N. López, M.T. M. Koper, Absence of CO_2 electroreduction on copper, gold and silver electrodes without metal cations in solution, Nat. Catal. 4 (2021) 654–662, https://doi.org/10.1038/s41929-021-00655-5.
[53] L. Zhang, H. Gong, Improvement in flexibility and volumetric performance for supercapacitor application and the effect of Ni-Fe ratio on electrode behaviour, J. Mater. Chem. A Mater. 3 (2015) 7607–7615, https://doi.org/10.1039/c4ta06649a.
[54] Z. Jovanovic, D. Bajuk-Bogdanović, S. Jovanović, Mravik, J. Kovač, I. Holclajtner-Antunović, M. Vujković, The role of surface chemistry in the charge storage properties of graphene oxide, Electro Acta 258 (2017) 1228–1243, https://doi.org/10.1016/j.electacta.2017.11.178.
[55] D.J.S. Sandbeck, M. Inaba, J. Quinson, J. Bucher, A. Zana, M. Arenz, S. Cherevko, Particle size effect on platinum dissolution: practical considerations for fuel cells, ACS Appl. Mater. Interfaces 12 (2020) 25718–25727, https://doi.org/10.1021/acsami.0c02801.
[56] D.J.S. Sandbeck, N.M. Secher, F.D. Speck, J.E. Sørensen, J. Kibsgaard, I. Chorkendorff, S. Cherevko, Particle size effect on platinum dissolution: considerations for accelerated stability testing of fuel cell catalysts, ACS Catal. 10 (2020) 6281–6290, https://doi.org/10.1021/acscatal.0c00779.
[57] S.T. Dix, S. Lu, S. Linic, Critical practices in rigorously assessing the inherent activity of nanoparticle electrocatalysts, ACS Catal. 10 (2020) 10735–10741, https://doi.org/10.1021/acscatal.0c03028.
[58] D. Sokaras, T.C. Weng, D. Nordlund, R. Alonso-Mori, P. Velikov, D. Wenger, A. Garachtchenko, M. George, V. Borzenets, B. Johnson, T. Rabedeau, U. Bergmann, A seven-crystal Johann-type hard x-ray spectrometer at the Stanford Synchrotron Radiation Lightsource, Rev. Sci. Instrum. 84 (2013), https://doi.org/10.1063/1.4803669.
[59] B. Ravel, M. Newville, ATHENA, ARTEMIS, HEPHAESTUS: Data analysis for X-ray absorption spectroscopy using IFEFFIT, : J. Synchrotron Radiat. (2005) 537–541, https://doi.org/10.1107/S0909049505012719.
[60] S. Calvin, XAFS for Everyone, CRC Press,, 2013, https://doi.org/10.1201/b14843.
[61] T.J.P. Hersbach, A.C. Garcia, T. Kroll, D. Sokaras, M.T.M. Koper, A.T. Garcia-Esparza, Base-accelerated degradation of nanosized platinum electrocatalysts, ACS Catal. 11 (2021) 9904–9915, https://doi.org/10.1021/acscatal.1c02468.
[62] C. Busó-Rogero, V. Grozovski, F.J. Vidal-Iglesias, J. Solla-Gullón, E. Herrero, J. M. Feliu, Surface structure and anion effects in the oxidation of ethanol on platinum nanoparticles, J. Mater. Chem. A Mater. 1 (2013) 7068–7076, https://doi.org/10.1039/c3ta10996h.
[63] N. Neha, T. Rafaïdeen, T. Faverge, F. Maillard, M. Chatenet, C. Coutanceau, Revisited mechanisms for glucose electrooxidation at platinum and gold nanoparticles, Electrocatalysis (2022), https://doi.org/10.1007/s12678-022-00774-y.
[64] J. Melke, A. Schoekel, D. Dixon, C. Cremers, D.E. Ramaker, C. Roth, Ethanol oxidation on carbon-supported Pt, PtRu, and PtSn catalysts studied by operando X-ray absorption spectroscopy, J. Phys. Chem. C. 114 (2010) 5914–5925, https://doi.org/10.1021/jp909342w.
[65] Y. Holade, H. Guesmi, J.S. Filhol, Q. Wang, T. Pham, J. Rabah, E. Maisonhaute, V. Bonniol, K. Servat, S. Tingry, D. Cornu, K.B. Kokoh, T.W. Napporn, S.D. Minteer, Deciphering the electrocatalytic reactivity of glucose anomers at bare gold electrocatalysts for biomass-fueled electrosynthesis, ACS Catal. (2022) 12563–12571, https://doi.org/10.1021/acscatal.2c03399.
[66] M.L. Toebes, Y. Zhang, J. Hájek, T. Alexander Nijhuis, J.H. Bitter, A. Jos Van Dillen, D.Y. Murzin, D.C. Koningsberger, K.P. De Jong, Support effects in the hydrogenation of cinnamaldehyde over carbon nanofiber-supported platinum catalysts: characterization and catalysis, J. Catal. 226 (2004) 215–225, https://doi.org/10.1016/j.jcat.2004.05.026.
[67] A.J. Plomp, H. Vuori, A.O.I. Krause, K.P. de Jong, J.H. Bitter, Particle size effects for carbon nanofiber supported platinum and ruthenium catalysts for the selective hydrogenation of cinnamaldehyde, Appl. Catal. A Gen. 351 (2008) 9–15, https://doi.org/10.1016/j.apcata.2008.08.018.
[68] R.W. Gosselink, R. Van Den Berg, W. Xia, M. Muhler, K.P. De Jong, J.H. Bitter, Gas phase oxidation as a tool to introduce oxygen containing groups on metal-loaded carbon nanofibers, Carbon N. Y 50 (2012) 4424–4431, https://doi.org/10.1016/j.carbon.2012.05.020.
[69] A.M. Führer, T. Van Haasterecht, N. Masoud, D.H. Barrett, T. Verhoeven, E. Hensen, C.B. Rodella, H. Bitter, The synergetic effect of support-oxygen groups and Pt particle size in the oxidation of α-D-glucose: a proximity effect in adsorption, ChemCatChemmCatChem (2022), https://doi.org/10.1002/cctc.202200493.
[70] L.M. Reid, T. Li, Y. Cao, C.P. Berlinguette, Organic chemistry at anodes and photoanodes, Sustain Energy Fuels 2 (2018) 1905–1927, https://doi.org/10.1039/c8se00175h.
[71] M.J. Bleda-Martínez, J.A. Maciá-Agulló, D. Lozano-Castelló, E. Morallón, D. Cazorla-Amorós, A. Linares-Solano, Role of surface chemistry on electric double layer capacitance of carbon materials, Carbon N. Y 43 (2005) 2677–2684, https://doi.org/10.1016/j.carbon.2005.05.027.
[72] X. Jiang, T. Shen, H. Li, L. Wang, Q. Yue, J. Liu, Effects of heat treatment temperature and atmosphere on electrocatalytic properties of platinum nanocrystals, J. Electroanal. Chem. 729 (2014) 53–60, https://doi.org/10.1016/j.jelechem.2014.06.028.
[73] L.G.R.A. Santos, K.S. Freitas, E.A. Ticianelli, Heat treatment effect of Pt-V/C and Pt/C on the kinetics of the oxygen reduction reaction in acid media, Electro Acta 54 (2009) 5246–5251, https://doi.org/10.1016/j.electacta.2009.03.078.
[74] F. Maillard, S. Schreier, M. Hanzlik, E.R. Savinova, S. Weinkauf, U. Stimming, Influence of particle agglomeration on the catalytic activity of carbon-supported Pt nanoparticles in CO monolayer oxidation, Phys. Chem. Chem. Phys. (2005) 375–383, https://doi.org/10.1039/b411377b.
[75] A.K. Datye, Q. Xu, K.C. Kharas, J.M. McCarty, Particle size distributions in heterogeneous catalysts: What do they tell us about the sintering mechanism? Catal. Today 111 (2006) 59–67, https://doi.org/10.1016/j.cattod.2005.10.013.
[76] A. Cuesta, A. Couto, A. Rincón, M.C. Pérez, A. López-Cudero, C. Gutiérrez, Potential dependence of the saturation CO coverage of Pt electrodes: The origin of the pre-peak in CO-stripping voltammograms. Part 3: Pt(poly), J. Electroanal. Chem. 586 (2006) 184–195, https://doi.org/10.1016/j.jelechem.2005.10.006.
[77] M.T.M. Garcıa, Gonzalo Koper, Stripping voltammetry of carbon monoxide oxidation on stepped platinum single-crystal electrodes in alkaline solution, Phys. Chem. Chem. Phys. 10 (2008) 3802–3811, https://doi.org/10.1039/b803503m.
[78] E.G. Ciapina, S.F. Santos, E.R. Gonzalez, Electrochemical CO stripping on nanosized Pt surfaces in acid media: a review on the issue of peak multiplicity, J. Electroanal. Chem. 815 (2018) 47–60, https://doi.org/10.1016/j.jelechem.2018.02.047.
[79] T.J.P. Hersbach, A.C. Garcia, T. Kroll, D. Sokaras, M.T.M. Koper, A.T. Garcia-Esparza, Base-accelerated degradation of nanosized platinum electrocatalysts, ACS Catal. 11 (2021) 9904–9915, https://doi.org/10.1021/acscatal.1c02468.
[80] X. Chen, I.T. McCrum, K.A. Schwarz, M.J. Janik, M.T.M. Koper, Co-adsorption of cations as the cause of the apparent pH dependence of hydrogen adsorption on a stepped platinum single-crystal electrode, Angew. Chem. - Int. Ed. 56 (2017) 15025–15029, https://doi.org/10.1002/anie.201709455.
[81] D. Ramaker, D. Koningsberger, The atomic AXAFS and Dl XANES techniques as applied to heterogeneous catalysis and electrocatalysis, Phys. Chem. Chem. Phys. 12 (2010) 5503–5513, https://doi.org/10.1039/b926434e.
[82] G. Moggia, T. Kenis, N. Daems, T. Breugelmans, Electrochemical Oxidation of d-Glucose in Alkaline Medium: Impact of Oxidation Potential and Chemical Side Reactions on the Selectivity to d-Gluconic and d-Glucaric Acid, ChemElectroChem 7 (2020) 86–95, https://doi.org/10.1002/celc.201901592.
[83] P. Parpot, P.R.B. Santos, A.P. Bettencourt, Electro-oxidation of d-mannose on platinum, gold and nickel electrodes in aqueous medium, J. Electroanal. Chem. 610 (2007) 154–162, https://doi.org/10.1016/j.jelechem.2007.07.011.
[84] Y.B. Vassilyev, O.A. Khazova, N.N. Nikolaeva, Kinetics and mechanism of glucose electrooxidation on different electrode-catalysts. Part I. Adsorption and oxidation on platinum, J. Electroanal. Chem. 196 (1985) 105–125, https://doi.org/10.1016/0022-0728(85)85084-1.
[85] A.M. Castro Luna, A.E. Bolzán, M.F.L. De Mele, A.J. Arvia, The voltammetric electrooxidation of organic residues produced from glucose electroadsorption on platinum electrodes with different preferred crystallographic orientations, Z. Fur Phys. Chem. 160 (1988) 25–43, https://doi.org/10.1524/zpch.1988.160.Part_1_2.025.
[86] K.D. Popović, A.V. Tripković, R.R. Adžić, Oxidation of d-glucose on single-crystal platinum electrodes: A mechanistic study, J. Electroanal. Chem. 339 (1992) 227–245, https://doi.org/10.1016/0022-0728(92)80454-C.
[87] A.M.C. Luna, A.E. Bolzán, M.F. de Mele, A.J. Arvia, The voltammetric electrooxidation of glucose and glucose residues formed on electrodispersed platinum electrodes in acid electrolytes, Pure Appl. Chem. 63 (1991) 1599–1608, https://doi.org/10.1351/pac199163111599.
[88] K. Popović, A. Tripković, N. Marković, R.R. Adžić, Structural effects in electrocatalysis: oxidation of glucose on single-crystal platinum electrodes, J. Electroanal. Chem. 295 (1990) 79–94, https://doi.org/10.1016/0022-0728(90)85007-R.
[89] K.B. Kokoh, J.M. Léger, B. Beden, C. Lamy, “On line” chromatographic analysis of the products resulting from the electrocatalytic oxidation of d-glucose on Pt, Au and adatoms modified Pt electrodes-Part I. Acid and neutral media, Electro Acta 37 (1992) 1333–1342, https://doi.org/10.1016/0013-4686(92)87004-J.
[90] D. Dixon, A. Habereder, M. Farmand, S. Kaserer, C. Roth, D.E. Ramaker, Space resolved, in operando X-ray absorption spectroscopy: Investigations on both the anode and cathode in a direct methanol fuel cell, J. Phys. Chem. C. 116 (2012) 7587–7595, https://doi.org/10.1021/jp211321u.
[91] Y. Kwon, K.J.P. Schouten, M.T.M. Koper, Mechanism of the Catalytic Oxidation of Glycerol on Polycrystalline Gold and Platinum Electrodes, ChemCatChem 3 (2011) 1176–1185, https://doi.org/10.1002/cctc.201100023.
[92] P. Kanninen, T. Kallio, Activation of commercial Pt/C catalyst toward glucose electro-oxidation by irreversible Bi adsorption, J. Energy Chem. 27 (2018) 1446–1452, https://doi.org/10.1016/j.jechem.2017.09.030.
[93] F. Largeaud, K.B. Kokoh, B. Beden, C. Lamy, On the electrochemical reactivity of anomers: electrocatalytic oxidation of α- and β-d-glucose on platinum electrodes in acid and basic media, J. Electroanal. Chem. 397 (1995) 261–269, https://doi.org/10.1016/0022-0728(95)04139-8.